Dalton Transactions

ROYAL SOCIETY OF CHEMISTRY

PAPER

View Article Online
View Journal | View Issue

Check for updates

Cite this: *Dalton Trans.*, 2024, **53**, 12301

Guest selectivity of [Ni_2] supramolecular helicates†

Manuel Imperato, [a,b,c] Alessio Nicolini, [a] Jordi Ribas-Ariño, [d] Michał Antkowiak, [c,e] Olivier Roubeau, [f] Andrea Cornia, *[a] Valentin Novikov, [c,g] Leoní A. Barrios *[c,g] and Guillem Aromí *[c,g]

Received 3rd June 2024,
Accepted 28th June 2024

DOI: 10.1039/d4dt01611d

rsc.li/dalton

Two new paramagnetic supramolecular helicates with the formula $(X@[Ni_2\mathbf{L}_3])^{3+}$ (X = Cl, or Br; **L** = a bis-pyrazolylpyridine ligand) have been prepared and are described. Helicates of this metal are very rare with virtually no prior examples of them acting as hosts of anionic species. The persistence of the new assemblies in solution has been demonstrated unambiguously by mass spectrometry and paramagnetic ^{1}H NMR. This has allowed us to establish the preference of the coordination [Ni_2] host for Cl^- over Br^-, in agreement with DFT calculations. These results show the promise of the use of metallohelicates as suitable systems for the selective encapsulation of specific anions in solution.

Introduction

The topic of anion recognition and manipulation is at the core of vibrant research activity, given the central role of such species in most biological and many industrial processes.[1–6] In most cases, the interaction with the receptor occurs *via* hydrogen bonds,[6–10] very often by encapsulation of the anionic species within a cage.[6,9,11–14] For most purposes, it is a major goal to identify stable host systems that present a defined selectivity for different types of anions.[14–16] A versatile family of cages is that of coordination supramolecular helicates,[17–21] which consist of self-assembled structures made of multitopic ligands acting as strands through their binding to two or more metal centers. In the case of bimetallic helicates, the metals act as nodes at each end of the structure while the strands often generate a central cavity where guests may be accomodated.[12,22,23] The size and symmetry of the encapsulated anions are in part defined and modulated by the number of strands as well as by the length and shape of the spacer between their coordinating units. We have been investigating a family of bis-pyrazolylpyridine ditopic ligands, such as **L**, shown in Fig. 1. These ligands predictably assemble with six-coordinate M(II) centers to form triple-stranded dinuclear cationic helicates, $[M_2\mathbf{L}_3]^{4+}$.[24–28] The N–H groups of **L** point towards the interior of the central cavity, which becomes ideal for the encapsulation of Cl^- and Br^- anions (X^-), producing $(X@[M_2\mathbf{L}_3])^{3+}$ host–guest supramolecular systems. This has been exploited in the case of M = Fe to modulate the spin switching properties of the $[Fe_2\mathbf{L}_3]^{4+}$ host.[25,29] If the spacer is made longer (*e.g.* replacing the central phenylene with biphenylene), the cavity becomes larger, and the host can then sequester bigger guests, such as transition metal complexes of the right symmetry.[30–32]

We present here new assemblies of Ni(II), **L** and halide anion guests, $(X@[Ni_2\mathbf{L}_3])^{3+}$ (X = Cl, Br), and produce experimental and theoretical evidence that their structure persists in

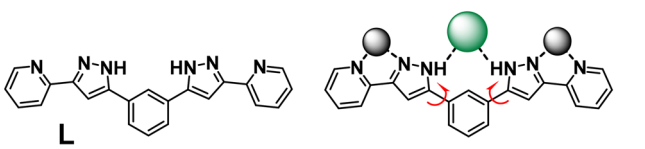

Fig. 1 (Left) Structure of the ligand 1,3-bis(3-(pyridin-2-yl)-1*H*-pyrazol-5-yl)benzene (**L**) and (right) coordination of **L** to metals (grey balls) through the pyrazolylpyridine moieties, highlighting the possible hydrogen bonds with a central anion like Cl^- or Br^- (green ball) and the conformational freedom arising from rotation about the indicated C–C bonds (red arrows).

[a]*Dipartimento di Scienze Chimiche e Geologiche e UdR INSTM, Università degli Studi di Modena e Reggio Emilia, via G. Campi 103, 41125 Modena, Italy. E-mail: acornia@unimore.it*
[b]*Dipartimento di Scienze Fisiche, Informatiche e Matematiche, Università degli Studi di Modena e Reggio Emilia, via G. Campi 213/A, 41125 Modena, Italy*
[c]*Departament de Química Inorgànica i Orgànica, Universitat de Barcelona, Diagonal 645, 08028 Barcelona, Spain. E-mail: aromi@ub.edu, leoni.barrios@ub.edu*
[d]*Departament de Química Física, Universitat de Barcelona, Diagonal 645, 08028 Barcelona, Spain*
[e]*Faculty of Physics, Adam Mickiewicz University, ul. Uniwersytetu Poznańskiego 2, 61-614 Poznań, Poland*
[f]*Instituto de Nanociencia y Materiales de Aragón (INMA), CSIC and Universidad de Zaragoza, Plaza San Francisco s/n, 50009 Zaragoza, Spain*
[g]*Institute of Nanoscience and Nanotechnology of the University of Barcelona (IN2UB), Barcelona, Spain*

†Electronic supplementary information (ESI) available: cif files, a PDF with crystallographic details, additional information on synthetic procedures, ESI-MS and NMR experiments, magnetic data treatment, and DFT calculations. CCDC 2343092 and 2343093. For ESI and crystallographic data in CIF or other electronic format see DOI: https://doi.org/10.1039/d4dt01611d

solution and that encapsulation of Cl^- is preferred over Br^-. This opens perspectives for the use of these types of coordination helicates as selective receptors of ions of relevance to environmental chemistry and other fields. The influence of the nature of the anion on the magnetic properties of the paramagnetic host is also briefly discussed.

Results and discussion

Synthesis and structures

Ligand **L** was prepared by a double Claisen condensation between 1,3-diacetylbenzene and 2-ethylpicolinate, followed by ring closure of β-diketone with hydrazine, according to a procedure slightly modified from that previously published by our group (see the ESI†).[25] The supramolecular host–guest systems $Cl@[Ni_2\mathbf{L}_3]Cl(BF_4)_2$ (**1**) and $Br@[Ni_2\mathbf{L}_3]Br_2(BF_4)$ (**2**) were then obtained as methanol/water solvates by self-assembly one-pot reactions between their various components. Thus, the addition of $^nBu_4NBF_4$ (TBABF$_4$) to a mixture of $NiCl_2{\cdot}6H_2O$ and **L** in MeOH produced crystals of **1**·3MeOH·4H$_2$O upon diffusion of Et_2O vapor. The same procedure starting from $Ni(BF_4)_2{\cdot}6H_2O$ and $^nBu_4NBr$ (TBABr) yields **2**·10MeOH·5H$_2$O (for simplicity, the compounds will be hereafter referred to as **1** and **2**). The identity and structure of the compounds were established by single-crystal X-ray diffraction (SCXRD, see below) and were consistent with data from microanalysis, electrospray ionization mass spectrometry (ESI-MS), and ^{1}H NMR (see below and the ESI†). It should be noted that the same **L**/Ni(II)/BF_4^-/X^- (X^- = Cl^- or Br^-) molar ratio (1.5/1/2/2) was used in both reactions. However, the BF_4^- and X^- anions are incorporated in different proportions in the structures of **1** and **2**, which are otherwise very similar. At 100 K (Table S1†), both compounds are found in the tetragonal non-centrosymmetric space group $I\bar{4}$ (Z = 8). The asymmetric unit of **1** comprises one supramolecular $(Cl@[Ni_2\mathbf{L}_3])^{3+}$ helicate (Fig. 2 and S1†), one Cl^- and two BF_4^- counterions, three molecules of MeOH and four molecules of H_2O. The Cl^- anion outside the cavity and one BF_4^- ion exhibit disorder over two positions with relative occupancies of 0.49 : 0.51 and 0.84 : 0.16, respectively. The asymmetric unit of **2** contains one $(Br@[Ni_2\mathbf{L}_3])^{3+}$ moiety (Fig. 2 and S2†), two Br^- and one BF_4^- species as counterions, together with ten and five solvate molecules of MeOH and H_2O, respectively. Here, one of the external Br^- anions is disordered over three positions (occupancies of 0.39 : 0.39 : 0.22). Elemental analysis revealed that the lattice MeOH molecules are partly replaced by H_2O upon exposure of these compounds to the atmosphere for some time. The supramolecular cation $(X@[Ni_2\mathbf{L}_3])^{3+}$ has almost the same structure in the two compounds (Fig. 2 and 3). It consists of a helicate where three **L** ligands act as strands, coordinating and bridging two Ni(II) ions through their pyrazolylpyridine chelating pockets, keeping them 9.663(3) and 9.7529(15) Å apart (for **1** and **2**, respectively). The hexacoordinated Ni(II) centers exhibit antiprismatic (pseudo-octahedral) coordination geometry, with Ni–N bond distances in the range of 2.060–2.176 Å. The proximity of this geometry to those of a perfect octahedron (OC-6 with O_h symmetry) and a perfect trigonal prism (TPR-6 with D_{3h} symmetry) was determined by means of continuous shape measures using the program SHAPE.[33] On average, the distances from the two reference polyhedra are 1.46 and 12.00, respectively, indicating that OC-6 is much closer to the observed geometry than TPR-6 (see individual values in Table S2†).

The local helical structure around the metals propagates throughout the molecule *via* the helical arrangement of the ligands. The latter is facilitated by the twisting around the C–C bonds that connect the central *m*-phenylene unit to the nearly planar pyrazolylpyridine groups (Fig. 1). The twisting angles are not uniform both within the same ligand and among different ligands. They range from 21.30° to 48.65° in **1** and from 25.8° to 42.82° in **2**, most likely reflecting solid-state packing effects and the interaction with the counterions outside the cavity. The two Ni(II) centers in the same molecule exhibit the same chirality and the crystal is consequently a racemic mixture of the enantiomeric species $\Delta\Delta(P)$ and $\Lambda\Lambda(M)$. The radius of the central cavity, defined as the average distance

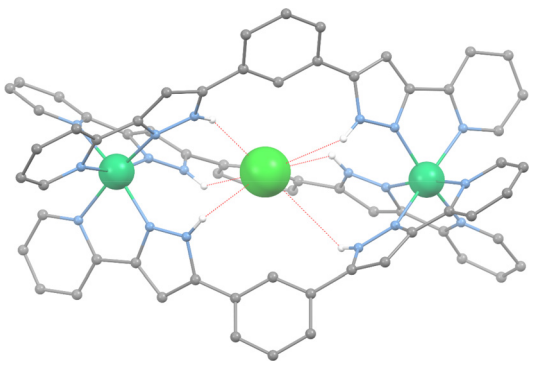

Fig. 2 Representation of the supramolecular cation $(Cl@[Ni_2\mathbf{L}_3])^{3+}$ of compound **1**. The large green ball is Cl, medium green balls are Ni, blue balls are N, grey balls are C and white balls are H. Only H atoms from N–H groups are shown. H-bonds are dashed red lines.

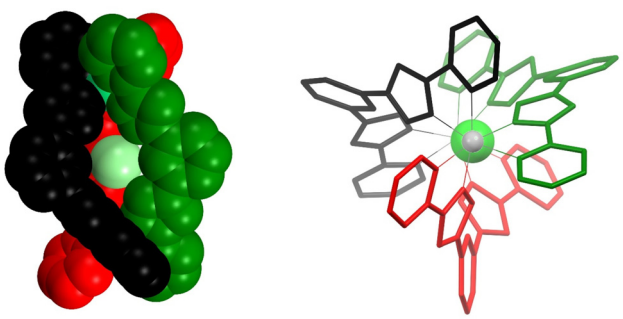

Fig. 3 (Left) Space-filling representation of the supramolecular cation $(Cl@[Ni_2\mathbf{L}_3])^{3+}$ of compound **1**, with ligands shown in red, green and black, respectively. (Right) View of the species $(Cl@[Ni_2\mathbf{L}_3])^{3+}$ along the Ni···Ni axis, emphasizing the helical arrangement engendered by the ligand twisting around the C–C bonds that connect the central *m*-phenylene unit to the pyrazolylpyridine groups.

between the three internal aromatic protons and their centroid, is 2.66 (in **1**) and 2.65 (in **2**) and is thus suited for the encapsulation of a Cl^- or a Br^- ion. The X^- guest is stabilized by six X···H–N hydrogen bonds with six pyrazolyl N–H groups pointing inside the cavity, describing approximately a trigonal antiprismatic geometry. These bonds are on average slightly shorter on one side of the antiprism (Tables 1 and S3, S4†). Therefore, the guest halide ion is closer to Ni2 than to Ni1 (with Ni···X distances, in the Cl/Br format, of 4.692/4.837 and 4.988/4.917 Å, respectively). The racemic $\Delta\Delta(P)$ and $\Lambda\Lambda(M)$ mixture in the solid mirrors the composition of the preexisting reaction mixture, which in turn originates from the degeneracy of the two equivalent processes of hexa-coordination around the Ni(II) ions (either with Δ or with Λ handedness), which ultimately define the configuration of the assembly. Once the assembly is formed, it should be locked in its final configuration unless a series of bond dissociations takes place. The interaction between the X^- anion and the host certainly contributes to the cementation of the structure (and its inertness). An alternative pathway of *P vs. M* interconversion without bond breaking seems very unlikely, since it would involve highly unstable non-chiral intermediates. The host–guest interaction would contribute to enhancing the energy barrier of this process. The remaining halide ions (whether disordered or not) are also found to form X···H–N hydrogen bonds from outside of the helicate with the ligand pyrazolyl groups, with H···X distances ranging from 2.094 to 2.162 Å for **1** and 2.461 to 2.913 Å for **2**.

Solution properties

The integrity of the supramolecular assemblies in MeCN solution was first studied with ESI-MS experiments (see the ESI†). Since the two compounds behave quite similarly (Fig. S3–S6†), the results are discussed together. Besides the expected signal attributed to the free ligand ($\mathbf{L} + H^+$), various peaks from the host–guest supramolecular assemblies present in the solid state were observed, specifically $(X@[Ni_2\mathbf{L}_3])^{3+}$, $(X@[Ni_2\mathbf{L}_3]\text{-}H^+)^{2+}$ and $(X@[Ni_2\mathbf{L}_3]BF_4)^{2+}$. Peaks deriving from the empty triple-stranded helicates, namely $([Ni_2\mathbf{L}_2]\text{-}2H^+)^{2+}$ and $([Ni_2\mathbf{L}_3]\text{-}2H^+)^{2+}$, were also observed, although such species were never detected in the solid state. These data strongly indicate that the helicates in **1** and **2**, together with their corresponding encapsulated guest, persist in the solution phase.

Table 1 List of N–H···X (X = Cl, **1**; Br, **2**) hydrogen bonding distances [Å] within **1** and **2**

N3H···Cl1	3.391[a]	N3H···Br1	2.947[a]
N4H···Cl1	3.342[a]	N4H···Br1	2.799[a]
N9H···Cl1	2.485[a]	N9H···Br1	2.932[a]
N10H···Cl1	2.586[a]	N10H···Br1	3.061[a]
N15H···Cl1	3.232[a]	N15H···Br1	2.911[a]
N16H···Cl1	2.684[a]	N16H···Br1	2.820[a]

[a] Distances are provided without an estimated standard deviation because the hydrogen atoms are placed in idealized positions and refined with a riding model.

The possible preference of the $[Ni_2\mathbf{L}_3]^{4+}$ host for one of the two guests (Cl^- or Br^-) was investigated by analyzing the ESI-MS response of MeCN solutions of **1** and **2** containing various amounts (1, 2, 3 or 10 eq.) of TBABr and $^nBu_4NCl$ (TBACl), respectively. To best serve this purpose, we focus on the spectral regions containing peaks from the $(X@[Ni_2\mathbf{L}_3])^{3+}$ species, as the latter give the most intense signals among the halogen-containing species. The conclusions extracted are however consistent with the observations made on the entire spectrograms. The presence of 1 eq. of TBABr in a solution of **1** leads to the formation of small amounts of $(Br@[Ni_2\mathbf{L}_3])^{3+}$ while producing a very slight decrease in the intensity of the $(Cl@[Ni_2\mathbf{L}_3])^{3+}$ signal (Fig. 4). Increasing amounts of added TBABr cause only very minor effects on the intensity of the generated $(Br@[Ni_2\mathbf{L}_3])^{3+}$ trace, while the $(Cl@[Ni_2\mathbf{L}_3])^{3+}$ peak from the original host–guest species is always found to dominate. Consequently, while some guest exchange is observed, Cl^- cannot be replaced by Br^-, even with a large excess of the latter. On the other hand, the addition of 1 eq. of TBACl to a solution of **2** leads to the formation of substantial amounts of $(Cl@[Ni_2\mathbf{L}_3])^{3+}$ together with a significant decrease in the $(Br@[Ni_2\mathbf{L}_3])^{3+}$ signal's intensity (Fig. 4). Larger amounts of TBACl lead to a further weakening of the signal from $(Br@[Ni_2\mathbf{L}_3])^{3+}$, which completely disappears in the presence of 10 eq. of the organic salt. These results show that while guest exchange may occur in both directions, Cl^- is clearly more favorably encapsulated than Br^-.

The solution properties were also investigated by NMR spectroscopy. The ^1H NMR spectrum of **1** in CD_3CN at room temperature exhibits nine peaks featuring paramagnetic shifts and broadening (Fig. 5). The spectrum is thus consistent with the idealized symmetry of the helicate observed in the solid state (D_3) and strongly suggests that this structure is preserved in solution. The signals were assigned based on the magnitudes of the paramagnetic shifts and linewidths, which are significantly larger for protons proximal to paramagnetic ions, as well as by comparison with previously reported complexes of

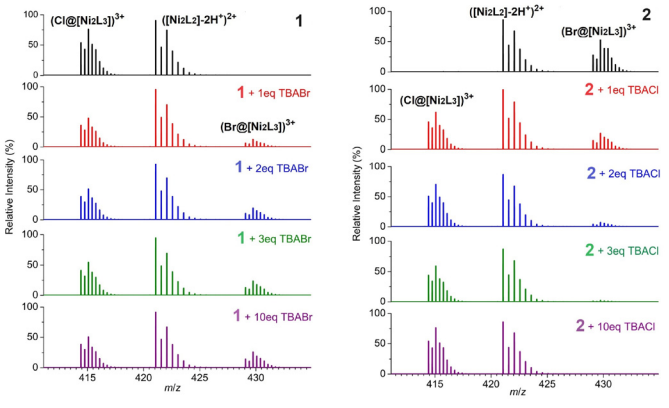

Fig. 4 Selected region (m/z = 411 to 435) of the ESI-MS spectrogram of compounds **1** (left) and **2** (right) before and after the addition of different amounts of TBABr and TBACl, respectively (direct infusion, MeCN, positive ion mode).

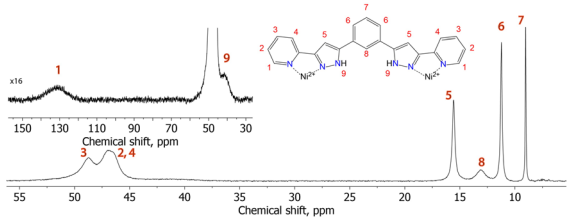

Fig. 5 ^{1}H NMR spectrum (500 MHz, 298 K) of a solution of compound **1** in CD_3CN with signal assignments.

the same ligand with iron(II) ions.[29] The spectrum of **2** is almost identical to that of **1** (Fig. S7†). The main difference is that the two broad peaks of pyridine β-protons, which are found between 46.5 and 47.0 ppm in **1**, merge into a unique signal at 46.5 ppm in **2**.

This marker was used to corroborate the favorable exchange of Br^- with Cl^- in MeCN solution observed in ESI-MS experiments (see above). The addition of approximately 3 eq. of TBACl to compound **2** dissolved in CD_3CN causes the expected splitting of the signal at 46.5 ppm (Fig. 6), proving that the guest Br^- ion in **2** is replaced by Cl^- and $(Cl@[Ni_2\mathbf{L}_3])^{3+}$ is formed. A large excess of TBACl (>10 eq.) causes the disappearance of the ^{1}H NMR signals and the precipitation of a solid phase, which is tentatively ascribed to a trihalide salt $X@[Ni_2\mathbf{L}_3]X_3$ (X^- = Br^- and/or Cl^-).

Solutions of **1** and **2** in CD_3CN were also examined by ^{35}Cl and ^{79}Br NMR. Unfortunately, when these quadrupolar nuclei (I = 3/2) are in non-symmetric environments, their NMR signals are broadened beyond detection. Compounds **1** and **2** are indeed ^{35}Cl and ^{79}Br silent, presumably because halide ions interact with the $[Ni_2\mathbf{L}_3]^{4+}$ helicate. Upon titration of a solution of **2** with TBACl, a ^{79}Br NMR signal becomes barely visible after the addition of 10 eq. of titrant and stands out more clearly as a larger excess of the organic salt is added (Fig. S8†). At the same time, however, precipitation of the helicate takes place (see above), meaning that only under these conditions are Br^- ions truly free in solution. The ^{35}Cl NMR spectra recorded during the titration show a similar trend, with a ^{35}Cl signal from truly free Cl^- ions being only observed after the addition of >10 eq. of TBACl (Fig. S9†). The titration of **1** with TBABr was also followed by ^{35}Cl and ^{79}Br NMR. No magnetic resonance signal from these nuclei was detected in the presence of small amounts of TBABr. A ^{79}Br signal was only observed upon the addition of 10 or more eq. of titrant, as the solid helicate started to precipitate, and its intensity increased as the titration proceeded (Fig. S10†). As a significant difference from reverse titration, however, a ^{35}Cl signal was never observed during the experiment (Fig. S11†). This means that all Cl^- ions available in the sample precipitate after a sufficient excess of Br^- ions is added, suggesting that the precipitate can be tentatively formulated as $Cl@[Ni_2\mathbf{L}_3]Br_2Cl$.

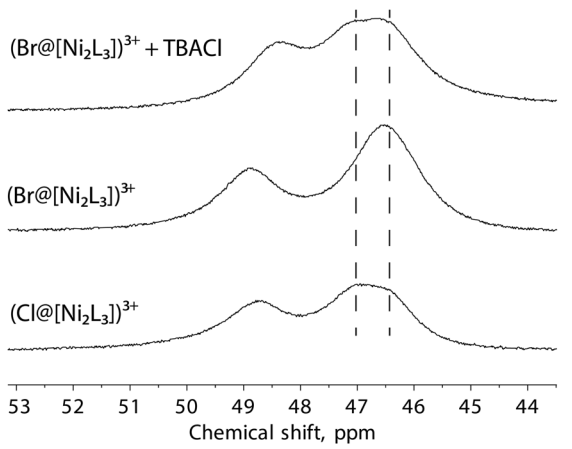

Fig. 6 Comparison of the ^{1}H NMR spectra (500 MHz, 298 K) of **1** (bottom), **2** (middle), and **2** + 3 eq. of TBACl (top) in CD_3CN. Dashed lines are a guide to the eye.

DFT calculations

The above-described experimental evidence that Cl^- is a preferred guest over Br^- was corroborated by density functional theory (DFT) calculations. Thus, the reaction DFT electronic energy (as obtained from the electronic Schrödinger equation) associated with the process in eqn (1) was evaluated after fully optimizing the geometry of reactants and products, using the polarizable continuum model to account for the influence of the solvent (MeCN) while including the effects of van der Waals interactions (see the ESI†).

$$(Br@[Ni_2\mathbf{L}_3])^{3+} + Cl^- \rightarrow (Cl@[Ni_2\mathbf{L}_3])^{3+} + Br^- \quad (1)$$

The calculated reaction energy is −16 kcal mol^{-1} and indicates that the guest replacement reaction is thermodynamically favoured, consistent with the observations made in ESI-MS and ^{1}H NMR experiments. The reason for this preference for Cl^- over Br^- is likely related to the general observation that the former usually establishes stronger hydrogen bonds than the latter.[34] Indeed, the calculated energy of the $X^-\cdots$H–N interaction between a halide anion and three pyrazolylpyridine moieties of a model complex $[Ni(\mathbf{L}_{cut})_3]^{2+}$ (Fig. S12†) in the gas phase is found to be 19.8 kcal mol^{-1} more favorable for Cl^- than for Br^-.

Magnetic properties

The effect of host–guest interactions on the solid-state magnetic properties of compounds **1** and **2** was probed through variable temperature bulk magnetic measurements. In view of the almost imperceptible influence of guest replacement on the ^{1}H NMR spectra, very little difference was expected. The $\chi_M T$ values of compounds **1** and **2** at 300 K amount to 2.37 and 2.59 cm^3 K mol^{-1}, respectively (χ_M is the molar paramagnetic susceptibility; Fig. S13†). In both cases, a plateau is observed down to approximately 15 K, where a small increase is detected, with maxima of 2.36 and 2.50 cm^3 K mol^{-1}, respectively. Upon further cooling, $\chi_M T$ declines sharply as a likely effect of Ni(II) single-ion magnetic anisotropy (extremely weak inter- and intramolecular interactions are anticipated).

Isothermal magnetization *vs.* field curves were also recorded at low temperature (Fig. S13†).

The magnetic behavior of both compounds was modeled using a single-ion zero-field splitting (zfs) plus Zeeman spin Hamiltonian, while neglecting any possible spin–spin interaction (see the ESI†). The two Ni(II) ions in each compound were assumed to have identical zfs tensors, described by the uniaxial (D) and rhombic (E) anisotropy parameters, as well as the same isotropic g factor. The best-fit parameters obtained analyzing both the susceptibility and magnetization curves were found to be similar or identical in the two compounds (Fig. S13†): in **1**, $D = -2.0$ K, $|E| = 0.1$ K, $g = 2.17$; in **2**, $D = -1.9$ K, $|E| = 0.1$ K, and $g = 2.22$.

Conclusions

The ditopic ligand 1,3-bis(3-(pyridin-2-yl)-1*H*-pyrazol-5-yl) benzene (**L**) spontaneously reacts in solution with Ni(II) and halide X^- ions (X = Cl, Br) to produce supramolecular host–guest cationic assemblies, $(X@[Ni_2\mathbf{L}_3])^{3+}$. Very importantly, these constructs persist in solution and can be detected, not only by paramagnetic NMR but also through mass spectrometry. This latter technique becomes essential to demonstrate the preference of Cl^- encapsulation with respect to Br^-, which is completely replaced by the former anion if added in a 10-fold excess. Interestingly, this selectivity is consistent with DFT calculations, where the influence of the MeCN solvent is taken into account.

Author contributions

The manuscript was written through contributions of all authors. All authors have given approval to the final version of the manuscript.

Data availability

The data supporting this article, including crystallographic details, information on synthetic procedures, ESI-MS and NMR experiments, magnetic data treatment, and DFT calculations, have been included as part of the ESI.†

Crystallographic data for compounds **1** and **2** have been deposited at the CCDC under 2343092 (**1**) and 2343093 (**2**).

Conflicts of interest

There are no conflicts to declare.

Acknowledgements

GA thanks the NextGenerationEU/PRTR-C17.I1 (from "Plan Complementario en Comunicación Cuántica" funded by Generalitat de Catalunya and the European Union) and Generalitat de Catalunya for the ICREA Academia 2023 prize. GA and OR thank the Spanish Ministry of Innovation for grants PID2020-118329RB-I00, PID2022-137764OB-I00, TED2021-129214B-I00 and BG22/00039. MI acknowledges the University of Modena and Reggio Emilia for awarding an outgoing mobility grant to the University of Barcelona. MA thanks the Polish National Science Centre for grant 2022/06/X/ST3/00108. This research used resources of the ALBA synchrotron.

References

1 N. H. Evans and P. D. Beer, *Angew. Chem., Int. Ed.*, 2014, **53**, 11716–11754.
2 P. A. Gale, E. N. W. Howe, X. Wu and M. J. Spooner, *Coord. Chem. Rev.*, 2018, **375**, 333–372.
3 L. K. Macreadie, A. M. Gilchrist, D. A. McNaughton, W. G. Ryder, M. Fares and P. A. Gale, *Chem*, 2022, **8**, 46–118.
4 P. E. Gale, E. N. W. Howe and X. Wu, *Chem*, 2016, **1**, 351–422.
5 P. Molina, F. Zapata and A. Caballero, *Chem. Rev.*, 2017, **117**, 9907–9972.
6 G. Picci, R. Montis, V. Lippolis and C. Caltagirone, *Chem. Soc. Rev.*, 2024, **53**, 3952–3975.
7 V. Amendola, L. Fabbrizzi and L. Mosca, *Chem. Soc. Rev.*, 2010, **39**, 3889–3915.
8 J. Zhao, D. Yang, X.-J. Yang and B. Wu, *Coord. Chem. Rev.*, 2019, **378**, 415–444.
9 S. O. Kang, M. A. Hossain and K. Bowman-James, *Coord. Chem. Rev.*, 2006, **250**, 3038–3052.
10 L. Liang, W. Zhao, X.-J. Yang and B. Wu, *Acc. Chem. Res.*, 2022, **55**, 3218–3229.
11 A. Peuronen, S. Forsblom and M. Lahtinen, *Chem. Commun.*, 2014, **50**, 5469–5472.
12 Q. Lin, L. Gao, B. Kauffmann, J. Zhang, C. Ma, D. Luo and Q. Gan, *Chem. Commun.*, 2018, **54**, 13447–13450.
13 L. J. Barbour, G. W. Orr and J. L. Atwood, *Nature*, 1998, **393**, 671–673.
14 R. Custelcean, P. V. Bonnesen, N. C. Duncan, X. Zhang, L. A. Watson, G. Van Berkel, W. B. Parson and B. P. Hay, *J. Am. Chem. Soc.*, 2012, **134**, 8525–8534.
15 P. J. Steel and D. A. McMorran, *Chem. – Asian J.*, 2019, **14**, 1098–1101.
16 A. Rajbanshi and R. Custelcean, *Supramol. Chem.*, 2012, **24**, 65–71.
17 M. Albrecht, *Chem. Soc. Rev.*, 1998, **27**, 281–288.
18 C. R. K. Glasson, L. F. Lindoy and G. V. Meehan, *Coord. Chem. Rev.*, 2008, **252**, 940–963.
19 C. Piguet, G. Bernardinelli and G. Hopfgartner, *Chem. Rev.*, 1997, **97**, 2005–2062.
20 M. Albrecht, *Eur. J. Inorg. Chem.*, 2020, **2020**, 2227–2237.
21 G. Aromí, H. Stoeckli-Evans, S. J. Teat, J. Cano and J. Ribas, *J. Mater. Chem.*, 2006, **16**, 2635–2644.

22 D. Zhang, Q. Gan, A. J. Plajer, R. Lavendomme, T. K. Ronson, Z. Lu, J. D. Jensen, B. W. Laursen and J. R. Nitschke, *J. Am. Chem. Soc.*, 2022, **144**, 1106–1112.
23 X.-S. Du, Y. Han and C.-F. Chen, *Chem. Commun.*, 2022, **58**, 1326–1329.
24 L. A. Barrios Moreno, N. Capó, H. Boulehjour, D. Reta, I. Tejedor, O. Roubeau and G. Aromí, *Dalton Trans.*, 2024, **53**, 7611–7618.
25 M. Darawsheh, L. A. Barrios, O. Roubeau, S. J. Teat and G. Aromí, *Chem. – Eur. J.*, 2016, **22**, 8635–8645.
26 R. Diego, A. Pavlov, M. Darawsheh, D. Aleshin, J. Nehrkorn, Y. Nelyubina, O. Roubeau, V. Novikov and G. Aromí, *Inorg. Chem.*, 2019, **58**, 9562–9566.
27 N. Capó, L. A. Barrios, J. Cardona, J. Ribas-Ariño, S. J. Teat, O. Roubeau and G. Aromí, *Chem. Commun.*, 2022, **58**, 10969–10972.
28 M. Estrader, J. Salinas Uber, L. A. Barrios, J. Garcia, P. Lloyd-Williams, O. Roubeau, S. J. Teat and G. Aromí, *Angew. Chem., Int. Ed.*, 2017, **56**, 15622–15627.
29 D. Y. Aleshin, R. Diego, L. A. Barrios, Y. V. Nelyubina, G. Aromí and V. V. Novikov, *Angew. Chem., Int. Ed.*, 2022, **61**, e202110310.
30 M. Darawsheh, L. A. Barrios, O. Roubeau, S. J. Teat and G. Aromí, *Angew. Chem., Int. Ed.*, 2018, **57**, 13509–13513.
31 L. A. Barrios, R. Diego, M. Darawsheh, J. I. Martínez, O. Roubeau and G. Aromí, *Chem. Commun.*, 2022, **58**, 5375–5378.
32 L. A. Barrios, S. J. Teat, O. Roubeau and G. Aromí, *Chem. Commun.*, 2023, **59**, 10628–10631.
33 S. Alvarez, D. Avnir, M. Llunell and M. Pinsky, *New J. Chem.*, 2002, **26**, 996–1009.
34 P. Sanchora, D. K. Pandey, D. Rana, A. Materny and D. K. Singh, *J. Phys. Chem. A*, 2019, **123**, 4948–4963.